Neutron interrogation of actinides with a 17 MeV electron accelerator and first results from photon and neutron interrogation non-simultaneous measurements combination

Adrien Sari, Frédérick Carrel, Frédéric Lainé, A. Lyoussi

Neutron interrogation of actinides with a 17 MeV electron accelerator and first results from photon and neutron interrogation non-simultaneous measurements combination

A. Sari[1], F. Carrel[1], F. Lainé[1], A. Lyoussi[2]

[1]CEA, LIST, Laboratoire Capteurs et Architectures Electroniques, 91191 Gif-sur-Yvette Cedex, France
[2]CEA, DEN, 13108 Saint-Paul-Lez-Durance Cedex, France

Corresponding author: adrien.sari@cea.fr
Telephone: +33 1 69 08 57 16
Fax: +33 1 69 08 60 30

Abstract

In this article, we demonstrate the feasibility of neutron interrogation using the conversion target of a 17 MeV linear electron accelerator as a neutron generator. Signals from prompt neutrons, delayed neutrons, and delayed gamma-rays, emitted by both uranium and plutonium samples were analyzed. First results from photon and neutron interrogation non-simultaneous measurements combination are also reported in this paper. Feasibility of this technique is shown in the frame of the measurement of uranium enrichment. The latter was carried out by combining detection of prompt neutrons from thermal fission and delayed neutrons from photofission, and by combining delayed gamma-rays from thermal fission and delayed gamma-rays from photofission.

Keywords

Electron accelerator; photoneutron; fission; photofission; uranium; plutonium

1. Introduction

Nuclear waste packages are characterized for management and repository purposes. One of the main steps of the characterization study consists in determining the amount of actinides (^{235}U, ^{239}Pu, ^{238}U, etc.) contained in packages. Active methods are often required as passive methods are usually not sufficient to quantify the latter. Two active methods enabling to induce fission reactions on actinides exist and differ in the type of irradiation beam employed. Neutron interrogation [1, 2] uses traditionally a deuterium-tritium neutron generator whereas photon interrogation [3-5] is based on the Bremsstrahlung photon beam produced with an electron accelerator. Photons can also react with heavy nuclei by photonuclear reactions and produce neutrons commonly referred to as photoneutrons. These particles are considered as interfering particles during photon interrogation. However, photoneutrons could be used as interrogative particles to carry out neutron interrogation which we investigate in this paper. In

addition to being an intense neutron source, an electron accelerator could therefore enable to combine several complementary techniques on a single measurement cell (photon interrogation, neutron interrogation, and high-energy imaging). Furthermore, combining results from neutron and photon non-simultaneous interrogations enables to obtain new information than that achieved individually by either of these two interrogations.

Other studies [6-11] mainly based on the use of low electron energy accelerator investigated the possibility of using the latter particles in different kinds of applications such as nuclear waste characterization or special nuclear material detection for homeland security. However, photoneutrons are usually produced in a secondary target made of heavy water or beryllium as photonuclear reaction thresholds are low in these two materials (respectively 2.2 MeV and 1.67 MeV). In a previous study [12], we showed that it is possible to carry out neutron interrogation of uranium samples using photoneutrons produced by the conversion target of an electron accelerator with few interfering high-energy photons. In this paper, new developments of our method are presented. In particular, we show the potential of this technique to measure and differentiate ^{235}U and ^{239}Pu. We also carried out the first combination of photon and photoneutron non-simultaneous interrogation measurements using a single electron accelerator. Such combination was applied to the measurement of uranium enrichment. First, we show theoretical formulas expressing signals of prompt neutrons, delayed neutron, and delayed gamma-rays. Then, we present our experiments and the setup on which we conducted the latter. Finally, experimental results are presented and discussed with the help of MCNPX simulations [13, 14].

2. Theoretical aspects

2.1 Prompt neutron signal

Theoretical prompt neutron signal (in counts) [1] can be expressed as

$$S_p = \tau_0 \, \nu_p \, \varepsilon_p \, (e^{-\lambda_c t_1} - e^{-\lambda_c t_2})/\lambda_c. \quad (1)$$

In the previous equation, τ_0 is the fission rate extrapolated at time origin (in fissions per second), ν_p the average number of prompt neutrons emitted per fission reaction, and ε_p the prompt neutron absolute detection efficiency, λ_c the neutron decay constant in the cell (per seconds), and $t_1$and t_2 respectively the prompt neutron counting time limits (in seconds).

By writing

$$f_p(t) = \left(e^{-\lambda_c t_1} - e^{-\lambda_c t_2}\right)/\lambda_c, \quad (2)$$

the prompt neutron signal (in counts) can be rewritten as

$$S_p = \tau_0 \, \nu_p \, \varepsilon_p \, f_p(t). \quad (3)$$

2.2 Delayed neutron signal

Theoretical delayed neutron signal (in counts) [1] can be written as

$$S_d = \tau_{fis}\, \nu_d\, \varepsilon_d \sum_{i=1}^{6} \beta_i / \lambda_i \left[1 - e^{-\lambda_i t_{irr}}\right] e^{-\lambda_i t_{cool}} \left[1 - e^{-\lambda_i t_{count}}\right] [(n+1)(1-\omega_i) - (1-\omega_i^{n+1})]/(1-\omega_i)^2, \quad (4)$$

with τ_{fis} is the fission rate (in fissions per second), ν_d the average number of delayed neutrons emitted per fission reaction, ε_d the delayed neutron absolute detection efficiency, β_i the delayed neutron fraction for the group i, λ_i the radioactive decay constant for group i (per second), t_{irr} is the pulse duration (in seconds), t_{cool} the cooling time (in seconds), t_{count} the counting time (in seconds), n the number of cycles, and $\omega_i = e^{-\lambda_i / f}$ with f being the frequency at which pulses are generated by the accelerator. More details about the theoretical expression of the delayed neutron signal can be found in the literature, as in [1].

By writing

$$f_d(t) = \sum_{i=1}^{6} \beta_i / \lambda_i \left[1 - e^{-\lambda_i t_{irr}}\right] e^{-\lambda_i t_{cool}} \left[1 - e^{-\lambda_i t_{count}}\right] [(n+1)(1-\omega_i) - (1-\omega_i^{n+1})]/(1-\omega_i)^2, \quad (5)$$

the delayed neutron signal (in counts) can be rewritten as

$$S_d = \tau_{fis}\, \nu_d\, \varepsilon_d\, f_d(t). \quad (6)$$

2.3 Delayed gamma-ray signal

Considering two nuclei, father and daughter (half-lives of precursor nuclides being short in comparison with the ones from father and daughter nuclides), theoretical delayed gamma-ray signal (in counts) [5] due to emission from daughter nuclide, can be written as

$$S(E_\gamma) = \tau_{fis}\, p_\gamma\, \varepsilon_\gamma\, t_{irr} \left\{ Y_i^d \left(\frac{1-e^{-n\lambda_d/f}}{1-e^{-\lambda_d/f}} \right) e^{-\lambda_d t_{cool}} \left(1 - e^{-\lambda_d t_{count}}\right) + Y_c^f \frac{\lambda_d}{\lambda_d - \lambda_f} \left[\left(\frac{1-e^{-n\lambda_f/f}}{1-e^{-\lambda_f/f}} \right) e^{-\lambda_f t_{cool}} \left(1 - e^{-\lambda_f t_{count}}\right) \right] - Y_c^f \frac{\lambda_f}{\lambda_d - \lambda_f} \left[\left(\frac{1-e^{-n\lambda_d/f}}{1-e^{-\lambda_d/f}} \right) e^{-\lambda_d t_{cool}} \left(1 - e^{-\lambda_d t_{count}}\right) \right] \right\}. \quad (7)$$

In the latter equation, τ_{fis} is the fission rate (in fissions per second), p_γ the gamma-ray emission probability, ε_γ the delayed gamma-ray absolute detection efficiency at energy E_γ, t_{irr} the pulse duration (in seconds), Y_i^d the independent yield of the daughter nuclide per thermal fission, Y_c^f the cumulative yield of the father nuclide per thermal fission, n the number of pulses, λ_d the radioactive decay constant of the daughter nuclide (per second), λ_f

the radioactive decay constant of the father nuclide (per second), f the pulse frequency (in Hz), t_{cool} is the cooling time (in seconds), t_{count} is the counting time (in seconds).

By writing

$$f_d = t_{irr}\left(\frac{1-e^{-n\lambda_d/f}}{1-e^{-\lambda_d/f}}\right)e^{-\lambda_d t_{cool}}\left(1-e^{-\lambda_d t_{count}}\right) \tag{8}$$

and

$$f_f = t_{irr}\frac{\lambda_d}{\lambda_d-\lambda_f}\left[\left(\frac{1-e^{-n\lambda_f/f}}{1-e^{-\lambda_f/f}}\right)e^{-\lambda_f t_{cool}}\left(1-e^{-\lambda_f t_{count}}\right)\right] - t_{irr}\frac{\lambda_f}{\lambda_d-\lambda_f}\left[\left(\frac{1-e^{-n\lambda_d/f}}{1-e^{-\lambda_d/f}}\right)e^{-\lambda_d t_{cool}}\left(1-e^{-\lambda_d t_{count}}\right)\right], \tag{9}$$

the delayed gamma-ray signal (in counts) can be rewritten as

$$S(E_\gamma) = \tau_{fis}\, p_\gamma\, \varepsilon_\gamma\, (Y_i^d f_d + Y_c^f f_f). \tag{10}$$

3. Experiments

Experiments were carried out at Saclay (France) with the electron accelerator of the SAPHIR facility [15] owned by CEA LIST. Electrons irradiated a 1 cm thick tantalum target of 99.9% purity. Mean energy of electron spectrum was 17 MeV and peak current was 100 mA with 2.5 µs pulse duration and 50 Hz repetition frequency. For this measurement campaign, we irradiated different uranium or plutonium certified samples which isotopic compositions were confirmed previously using IGA code [16]. We used eight samples: four samples of uranium enriched between 2.8% and 9.6%; and four plutonium samples containing either 74.6% or 90.0% of ^{239}Pu. Two other samples were retained as reference samples because of their high levels in ^{235}U or ^{239}Pu: a uranium sample enriched at 85% in ^{235}U and a plutonium sample at 94% of ^{239}Pu (PIDIE sample [17]). All samples were irradiated in a neutron interrogation cell which is represented in Fig. 1. Fast photoneutrons emitted by the conversion target were thermalized by 10 cm thick polyethylene walls in order to maximize the fission rate in the sample [12]. Fission neutrons were measured with ^{3}He detectors. Each neutron detection block contains three ^{3}He detectors (150NH100) embedded in polyethylene and is surrounded by cadmium. Two blocks were positioned one on the top of the other against both sides of the cell, as shown on Fig. 1. A trigger enabled to synchronize our neutron detection system with the accelerator pulses.

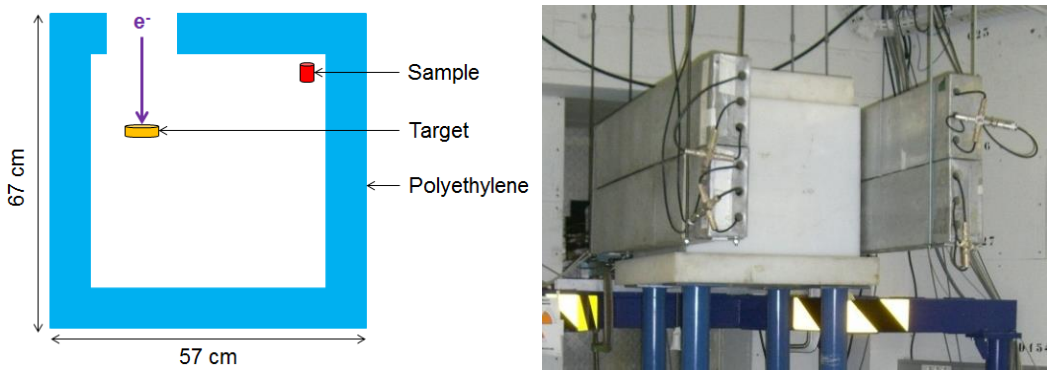

Fig. 1. Scheme and photography of a neutron cell based on an electron accelerator.

First, we placed the sample perpendicularly from the target at a distance of 30 cm. Sample was positioned outside the high-energy photon beam in order to avoid spurious photofission reactions during measurement. Prompt and delayed neutrons emitted by the sample were detected during the 10 min long irradiation. Prompt neutrons were detected between 3 ms and 8 ms after the pulse and delayed neutrons between 10 ms and 20 ms. By way of illustration, Fig. 2 superimposes an example of signal obtained for the plutonium reference sample, with and without a cadmium cover, and active background noise, whereas Fig. 3 shows results obtained for samples of different ^{235}U masses (139 mg, 311 mg, and 764 mg).

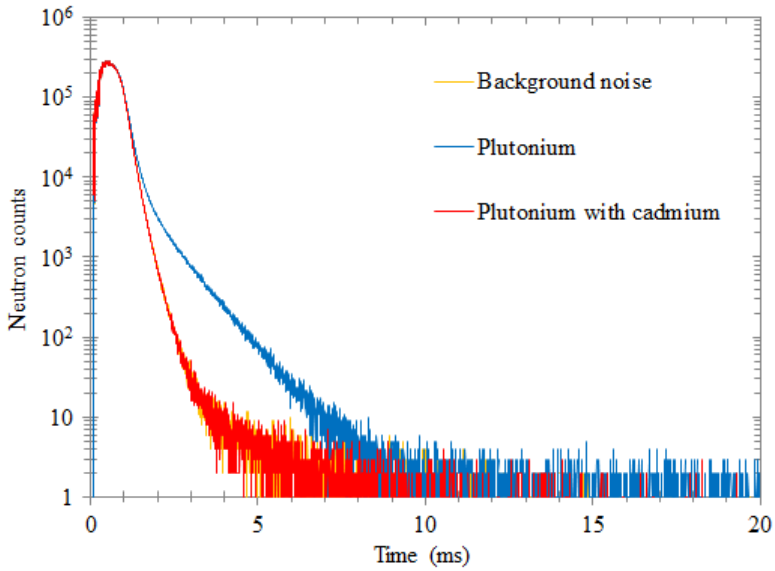

Fig. 2. Example of signals obtained after 10 min irradiation for the plutonium reference sample with and without cadmium.

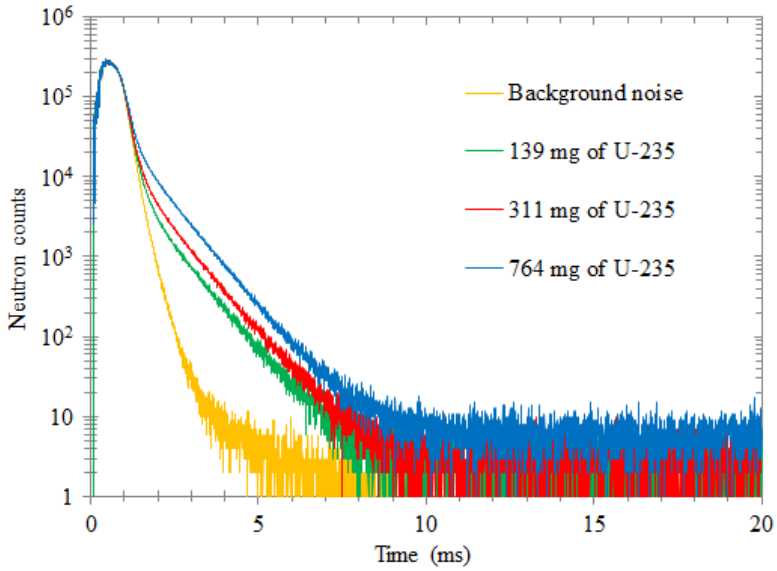

Fig. 3. Example of signals obtained after 10 min irradiation for uranium samples of different ^{235}U masses.

After 5 min of cooling time, we removed the sample from the cell and placed the latter in front of a germanium detector, as shown in Fig. 4. We used a p-type GEM40P-PLUS HPGe detector, which presents 40% relative efficiency, linked to a DSPECPro digital gamma-ray spectrometer, both made by ORTEC. Delayed gamma-rays were detected during 10 min while the sample was positioned at 15 cm distance from the front of the germanium detector. For plutonium samples, a 1 mm thick cadmium foil was placed between the sample and the HPGe detector in order to reduce impact of 59 keV gamma-ray emitted by ^{241}Am, and therefore minimize the dead time value.

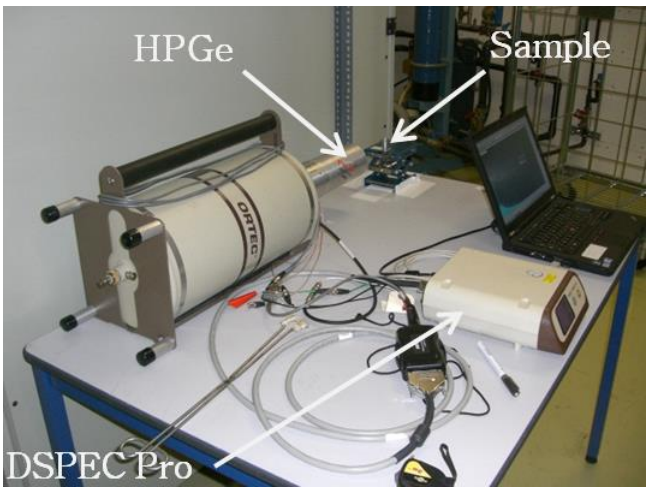

Fig. 4. Acquisition of delayed gamma-ray spectra with a germanium detector.

Then, we removed the neutron cell and carried out photon interrogation of the sample. This time, samples were placed in front of the conversion target in order to be mainly irradiated by high-energy photons during 10 min. Delayed neutrons were detected during the irradiation by the same detection blocks as the ones used for the previous interrogation. Two blocks were positioned at each side of the sample. Distance between the sample and a detection block was

62 cm whereas the one between the sample and the conversion target was 56 cm. After the irradiation, the sample was removed and placed in front of the HPGe detector. Delayed gamma-rays were measured using same protocol as the one given previously.

4. Results and discussion

Neutron counting results presented in this section were acquired with a single neutron detection block containing three ^{3}He detectors. For each signal, we subtracted active and passive background noises from the facility. For measurements carried out with plutonium, passive emission from the samples was also taken into account. On each figure, error bars on statistical uncertainties at one sigma are only presented if the latter are bigger than symbols.

4.1 Neutron interrogation measurements

4.1.1 Prompt and delayed neutron signals

Prompt and delayed neutron signals were studied during three different measurement campaigns. The latest results obtained with the eight standard samples presented previously are shown in Fig. 5 and Fig. 6. Signal increases linearly with ^{235}U or ^{239}Pu mass, as expected by theory. However, one can notice that curves do not go through the origin of the graphic which we investigated.

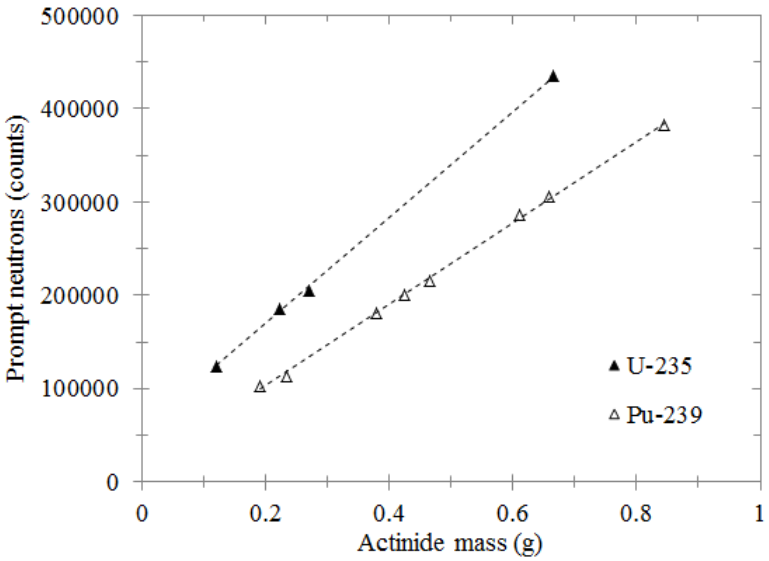

Fig. 5. Prompt neutron signal versus ^{235}U or ^{239}Pu mass.

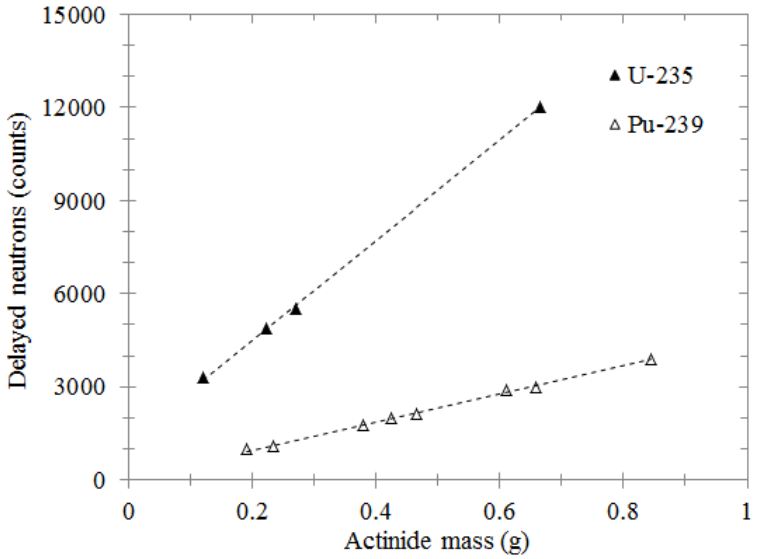

Fig. 6. Delayed neutron signal versus ^{235}U or ^{239}Pu mass.

Comparison between measurements conducted with and without cadmium cover around the samples enabled to quantify effect of fast fission and photofission reactions on fertile isotopes, contained in the uranium or plutonium samples, to the prompt and delayed neutron signals measured. We found that these reactions account for less than 0.2% of the prompt neutron signals, and between 4% and 14% of the delayed neutron signals. However, MCNPX simulations showed that contribution from photofission reactions is low in comparison with the one of fast fission reactions. We have also verified by simulation that contribution of self-interrogation of the samples (fast fission reactions on fertile isotopes induced by prompt neutrons emitted further to thermal fission reactions on fissile isotopes) is negligible. Furthermore, for plutonium samples, we conducted MCNPX simulations to quantify contribution of thermal fission reactions on ^{241}Pu to the ^{239}Pu signal measured. The impact of this contribution accounts for less than 1% of the signal due to the low amount of ^{241}Pu in these samples. Finally, we concluded that offsets of the curves can mainly be attributed to self-protection of the samples (interrogation of the fissile mass contained in samples is limited to its external part). MCNPX simulations enabled to confirm this assumption. One can notice that self-protection is stronger for our measurements conducted with uranium than for the ones carried out with plutonium. This is due to the fact that, for a same mass of actinide, irradiation of uranium was carried with a single sample contrary to measurements conducted for plutonium. Indeed, different combinations of plutonium samples were required to irradiate a wider range of ^{239}Pu masses. Furthermore, it is important to emphasize that, for same mass of actinide, signal obtained for uranium is higher than the one obtained for plutonium because of strong self-absorption in our plutonium samples (absorption of neutrons in the non-fissile mass contained in samples).

4.1.2 Ratio between prompt and delayed neutron signals

We determined the ratio between prompt and delayed neutron signals for experiments carried out for both uranium and plutonium. Measurements were carried out for two types of samples:

the standard samples mentioned previously and reference samples. Fig. 7 presents respectively results for the standard samples. Mean values of the ratios, independent of actinide mass, are about 37.35 and 101.65 respectively for uranium and plutonium. Experiments conducted with the uranium and plutonium reference samples lead respectively to the following values: 32.83 and 98.52. Ratio between average numbers of prompt and delayed neutrons emitted depends on the type of actinide which follows the fission reaction. However, measured ratios depend on many experimental parameters, as illustrated by equations 3 and 6, and can therefore not be directly compared to the theoretical mean numbers of prompt and delayed neutrons emitted by ^{235}U or ^{239}Pu.

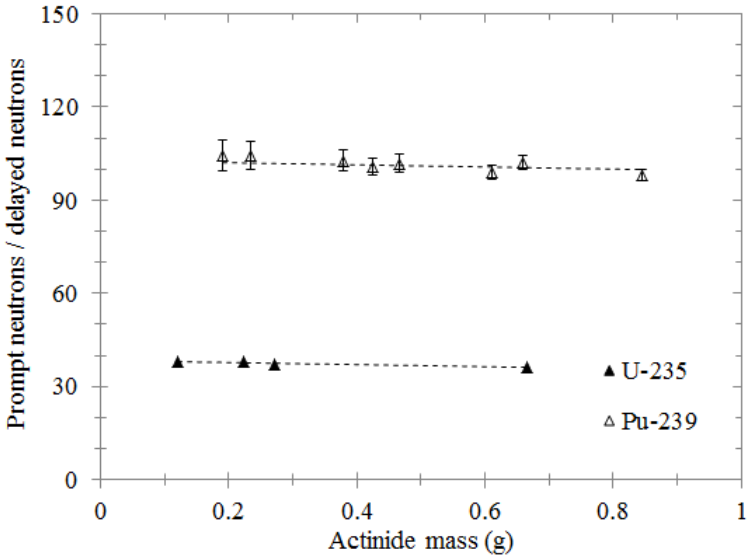

Fig. 7. Ratio between prompt and delayed neutron signals versus ^{235}U or ^{239}Pu mass.

We calculated the ratios between the prompt and delayed signals for both ^{235}U and ^{239}Pu, and compared results obtained with our experimental values. In order to simplify the fission rate (τ_{fis}) in these calculations, the fission rate extrapolated at time origin (τ_0) in equation 3 was expressed using the following approximation: $\tau_0 = n\,\lambda_c\,t_{irr}\tau_{fis}$. In such a way, we consider that the fission rate is at its highest value at time origin and decreases over time according to the neutron decay constant (λ_c). In reality, the fission rate reaches its maximal value at after a few hundreds of microseconds necessary for fast photoneutrons emitted by the target to be thermalized in the cell. However, we have verified by MCNPX simulation that this approximation can be done in the frame of these experiments (taking into account a correction factor of 1.15 on the delayed signal). Value of the neutron decay constant in the cell (λ_c) was deduced from exponential decay of the prompt neutron signal measured. The prompt and delayed neutron detection efficiencies (ε_p and ε_d respectively) were measured using ^{252}Cf and ^{241}AmLi sources. The average number of prompt neutrons emitted following thermal fission on ^{235}U and ^{239}Pu were taken from [18] (respectively 2.42 and 2.87 prompt neutrons) and delayed neutron parameters were taken from [19]. Finally, calculations lead to the following ratios: 31.87 for ^{235}U and 98.54 for ^{239}Pu. Measured ratios are compared with calculated ones in Table 1. Each comparison is made twice: with and without subtraction of the part of the signal due to fast fission and photofission reactions for the signal determined by measurement

(by comparison between measurements carried with and without the cadmium sleeve around the sample). Ratios determined by calculation do not take contribution of these two types of reactions or self-interrogation into account.

	Without correction	With correction
Uranium samples	1.02	1.09
Uranium, reference sample	0.90	0.97
Plutonium samples	0.90	-
Plutonium, reference sample	0.87	0.90

Table 1. Comparison of measured and calculated ratios between the prompt and delayed neutron signals, with and without fast fission and photofission impact subtracted in measured ratios.

Ratios between prompt and delayed neutron signals, obtained by experiment or calculation, are overall in good agreement. Moreover, we can notice that subtraction of the part of the signal measured due to fast fission and photofission reactions diminishes the gap between experiment and calculation for the reference samples. Furthermore, as detection efficiencies used in the calculated ratios (ε_p and ε_d) were measured with punctual sources, correction factors taking into account mass, density, and geometry of the samples could potentially help reducing the gap between calculations and measurements. Finally, these results enable to achieve good confidence in the fact that sample interrogation is mainly due to thermal photoneutrons.

4.1.3 Delayed gamma-ray signal

We focused on four intense peaks of delayed gamma-rays emitted by four different fission products following uranium fission, the same peaks on which we drew attention in a previous study [12]: ^{89}Rb (1031.9 keV), ^{94}Y (918.7 keV), ^{131}Sb (943.4 keV), and ^{138}Xe (1768.3 keV). Fig. 8 shows evolution of the net peak areas with ^{235}U mass for each delayed gamma-ray studied. The signal measured increases linearly with ^{235}U mass. As well as for prompt and delayed neutron signals, self-protection of the samples explains why curves do not go through the origin of the graphic. However, slopes of the four curves vary from one line to the other. This is due to the fact that, for each delayed gamma-ray considered, values of the following parameters differ: cumulative yields from thermal fission of ^{235}U, gamma-ray emission probabilities, and absolute detection efficiencies.

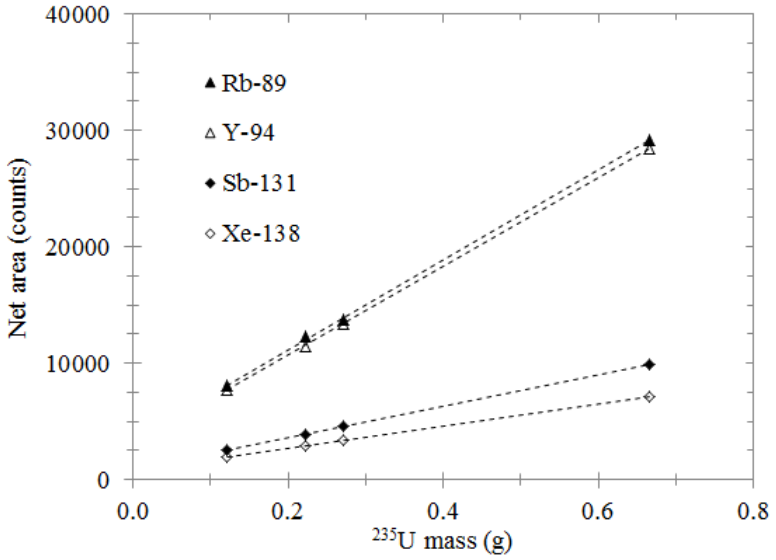

Fig. 8. Delayed gamma-ray signal versus ^{235}U mass.

Accurate analysis of the delayed-gamma-ray signals enables to achieve more information on the interrogation of the sample than that obtained previously with the prompt and delayed neutron signals. As half-life time of daughter nuclide is considerably longer than that of its direct precursor, analysis of the net peak area leads to the cumulative yield of the daughter nuclide [20]. If we assume that the absolute detection efficiency is similar at the gamma-ray energies of 918.7 keV and 943.4 keV, the theoretical ratio between the slopes of the curves obtained for ^{94}Y and ^{131}Sb is therefore given by the following equation:

$$R_{\frac{94_Y}{131_{Sb}}} = \frac{p_{\gamma,94_Y}\ Y^d_{c,94_Y}\ f_{d,94_Y}}{p_{\gamma,131_{Sb}}\ Y^d_{c,131_{Sb}}\ f_{d,131_{Sb}}}.$$

Values of emission probabilities for the two gamma-rays of interest ($p_{\gamma,94_Y}$ and $p_{\gamma,131_{Sb}}$) were found in the nuclear data library JEFF-3.1.1. We took the values of the cumulative yields of the daughter nuclides per thermal fission ($Y^d_{c,94_Y}$ and $Y^d_{c,131_{Sb}}$) measured by F. Carrel *et al.* [20]. Temporal functions ($f_{d,94_Y}$ and $f_{d,131_{Sb}}$) were calculated from equations 6 and 8 taking into account values of ^{94}Y and ^{131}Sb half-life times taken in the Nubase 2003 evaluation. Finally, the value of the theoretical ratio is 2.810. Since the ratio between the slopes of the curves obtained by experiment for ^{94}Y and ^{131}Sb is 2.807, theory and measurements are in very good agreement. The signal measured is characteristic from ^{235}U thermal fission and confirms our previous conclusions obtained further to the prompt and delayed neutron signals analysis: samples irradiated in the neutron cell undergo thermal fission.

4.2 Combination of photon and neutron interrogation non-simultaneous measurements

4.2.1 Prompt neutrons from thermal fission and delayed neutrons from photofission

Thermal neutrons interrogate fissile isotopes whereas high-energy photons interrogate both fissile and fertile isotopes. Combination of photon and neutron separate interrogations could therefore be a new approach for the measurement of uranium enrichment. Three uranium samples of same total mass and enriched between 2.8% and 6.2% were used for these first tests. Fig. 9 presents experimental results obtained. We can see that the ratio increases with the enrichment, which is in agreement with theory. Similar results were found by detecting delayed neutrons from thermal fission instead of prompt neutrons, as shown in Fig. 10.

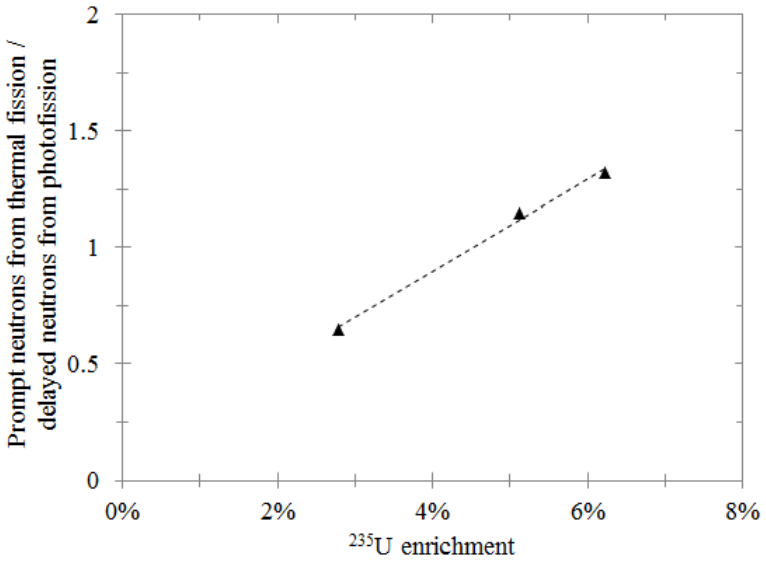

Fig. 9. Ratio between signals of prompt neutrons from thermal fission and delayed neutrons from photofission, obtained for three uranium samples of various enrichments in ^{235}U.

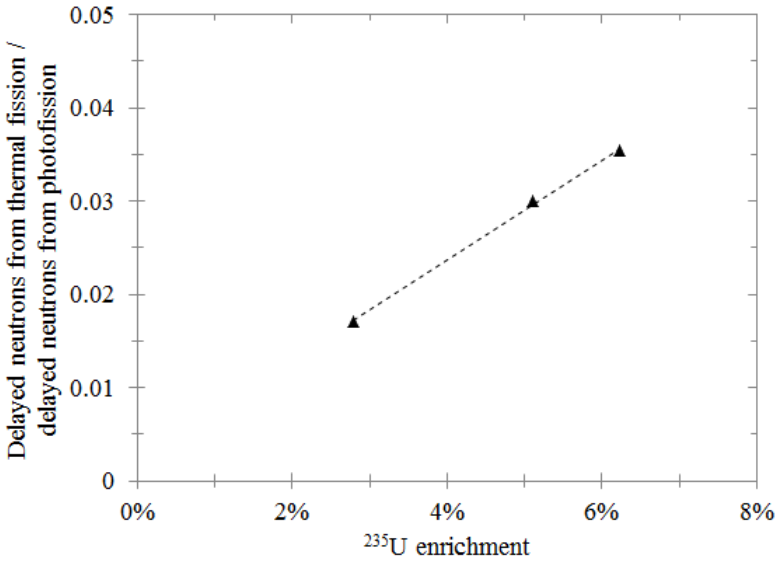

Fig. 10. Ratio between signals of delayed neutrons from thermal fission and delayed neutrons from photofission, obtained for three uranium samples of various enrichments in ^{235}U.

4.2.2 Delayed gamma-rays from thermal fission and delayed gamma-rays from photofission

In order to confirm the latter results, Fig. 11 presents ratios between net peak areas extracted from thermal fission and photofission delayed gamma-ray spectra. The ratio increases with uranium enrichment. However, lines do not overlap and have different intercepts and slopes as the following parameters are different for each curve: fission product yields, delayed gamma-ray emission probabilities, and absolute detection efficiencies.

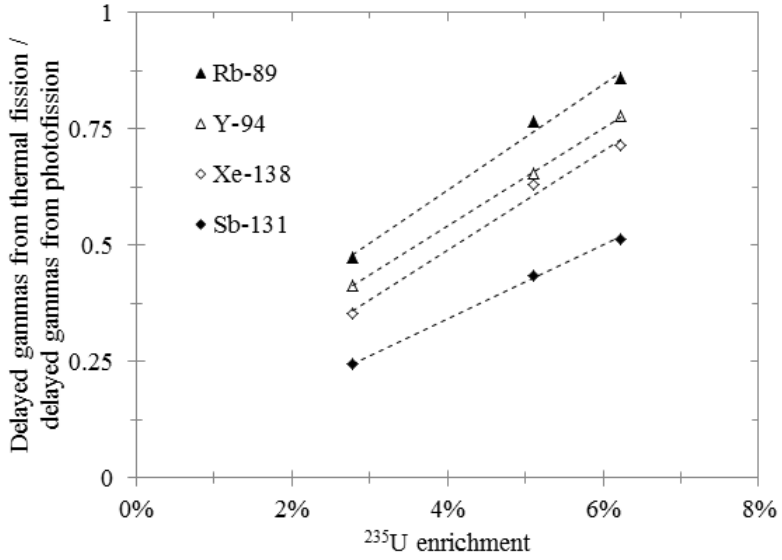

Fig. 11. Ratio between signals of delayed gamma-rays from thermal fission and delayed gamma-rays from photofission, obtained for three uranium samples of various enrichments in ^{235}U.

5. Summary

We investigated the potential of an electron accelerator to be used as a multi-device mean on a platform dedicated to nuclear waste drums characterization. We carried out neutron interrogation of uranium and plutonium samples in a cell using photoneutrons emitted by a 17 MeV electron accelerator as interrogative particles. Different types of experiments enabled to confirm that the neutron flux is largely thermal in the cell. We also presented the first combination of photon and photoneutron separate interrogation measurements using a single electron accelerator. This combination, applied successfully to the measurement of uranium enrichment, opens up new and interesting horizons for research on nuclear waste characterization that should be further investigated.

Furthermore, mass detection limits of the neutron interrogation measurement were calculated from the prompt neutron signals. About 7 mg of ^{235}U and 12 mg of ^{239}Pu can be detected in 150 seconds. An optimized neutron detection system, offering shorter neutron half-life time in the detection blocks, would allow detecting prompt neutrons earlier and expand mass detection limits. In order to further evaluate our method, an optimized neutron interrogation cell based on an electron accelerator will be designed by simulation with the objective of carrying out measurements on 220 liter nuclear waste drums.

References

[1] A.-C. Raoux, A. Lyoussi, C. Passard, C. Denis, J. Loridon, J. Misraki, P. Chany, Nucl. Instr. Meth. B 207 (2003) 186
[2] A. Mariani, C. Passard, F. Jallu, H. Toubon, Nucl. Instr. Meth. B 211 (2003) 389
[3] A. Lyoussi, J. Romeyer-Dherbey, F. Jallu, E. Payan, A. Buisson, G. Nurdin, J. Allano, Nucl. Instr. Meth. B 160 (2000) 280
[4] M. Gmar, F. Jeanneau, F. Lainé, H. Makil, B. Poumarède, F. Tola, Appl. Radiat. Isot. 63 (2005) 613
[5] F. Carrel, M. Agelou, M. Gmar, F. Lainé, J. Loridon, J.-L. Ma, C. Passard, B. Poumarède, IEEE Trans. Nucl. Sci. 57 (2010) 2862
[6] L.A. Franks, J.L. Pigg, J.T Caldwell, M.R. Cates, W.E. Kunz, B.W. Noel, D.A. Close, Nucl. Instr. Meth. 192 (1982) 571
[7] V.L. Chakhlov, Z.W. Bell, V.M. Golovkov, M.M. Shtein, Nucl. Instr. Meth. A 422 (1999) 5
[8] F. Jallu, A. Lyoussi, C. Passard, E. Payan, H. Recroix, G. Nurdin, A. Buisson, J. Allano, Nucl. Instr. Meth. B 170 (2000) 489
[9] J.L. Jones, W.Y. Yoon, D.R. Norman, K.J. Haskell, J.M. Zabriskie, S.M. Watson, J.W. Sterbentz, Nucl. Instr. Meth. B 241 (2005) 770
[10] Y. Yang, Y. Li, H. Wang, T. Li, B. Wu, Nucl. Instr. Meth. A 579 (2007) 400
[11] L. Lakosi, C. Tam Nguyen, J. Bagi, Nucl. Instr. Meth. B 266 (2008) 295
[12] A. Sari, F. Carrel, M. Gmar, F. Lainé, A. Lyoussi, S. Normand, IEEE Trans. Nucl. Sci. 59 (2012) 605
[13] J.F. Briesmeister, Los Alamos National Laboratory Report LA-13709-M (2000)

[14] J.S. Hendricks, Los Alamos National Laboratory Report LA-UR-04-0570 (2004)
[15] F. Carrel, M. Agelou, M. Gmar, F. Lainé, B. Poumarède, B. Rattoni, IEEE Trans. Nucl. Sci. 57 (2010) 3687
[16] A.-C. Simon, F. Carrel, I. Espagnon, M. Lemercier, A. Pluquet, IEEE Trans. Nucl. Sci. 58 (2011) 378
[17] J. Morel, M. Bickel, C. Hill, A. Verbruggen, Appl. Radiat. Isot. 60 (2004) 607
[18] Database ENDF/B.VII.1 [online]. Available at: http://www.nndc.bnl.gov/exfor/endf.htm
[19] R.W. Waldo, R.A. Karam, R.A. Meyer, Phys. Rev. C 23 (1981) 1113
[20] F. Carrel, M. Agelou, M. Gmar, F. Lainé, J. Loridon, J.-L. Ma, C. Passard, B. Poumarède, IEEE Trans. Nucl. Sci. 58 (2011) 2064

Acknowledgments

The authors are very grateful to Dr. C. Passard for fruitful discussions on neutron interrogation.